Whitmarsh, R.B., Sawyer, D.S., Klaus, A., and Masson, D.G. (Eds.), 1996
Proceedings of the Ocean Drilling Program, Scientific Results, Vol. 149

23. GEOCHEMISTRY OF SERPENTINIZED MANTLE PERIDOTITE FROM SITE 897 IN THE IBERIA ABYSSAL PLAIN[1]

Karl Seifert[2] and Dale Brunotte[2]

ABSTRACT

Serpentinized mantle peridotites from Site 897 are highly variable in composition and mineralogy, ranging from lherzolites to harzburgites and, more infrequently, to dunites. Lherzolites are enriched in Al_2O_3, TiO_2, CaO, Cr_2O_3 and rare-earth elements relative to harzburgites and dunites, which are enriched in MgO and NiO. Texturally some of the lherzolites are characterized by mylonitic bands of fine-grained plagioclase, clinopyroxene, orthopyroxene, and olivine between larger crystals of olivine, orthopyroxene, clinopyroxene, plagioclase, and chrome spinel. These textural characteristics suggest the lherzolites have been enriched by intrusion of basaltic magma. Moreover, some of the lherzolites have flat rare-earth-element patterns near chondritic abundance, and regarded as typical of primitive mantle, whereas others have rare-earth-element patterns similar to normal mid-ocean ridge basalt, suggesting metasomatic enrichment by the addition of a normal mid-ocean ridge basaltic magma. The vertical and lateral heterogeneity of mantle peridotites at Site 897 shows that the mantle can be locally heterogeneous and that modeling of the mantle as a few layers of relatively homogeneous material represents a vast oversimplification that has no significance at the local level.

INTRODUCTION

Ocean Drilling Program (ODP) Leg 149 explored the ocean-continent transition (OCT) on the Iberia Abyssal Plain and its role in the opening of the Atlantic Ocean approximately 130 Ma. Leg 149 was the first of several legs in the Atlantic Ocean to study rifted-margin formation and evolution. Transects were chosen across both volcanic and nonvolcanic conjugate rifted margins, with basement being the major drilling target. The Iberia Abyssal Plain was chosen as the best defined nonvolcanic rifted margin on the eastern edge of the Atlantic Ocean (Fig. 1). The geologically conjugate Newfoundland margin was to be drilled on a later leg. The Iberia continental margin consists of several topographically distinct regions. In the northern part of the margin, continental crust extends seaward under shallow water as the 200 km by 150 km Galicia Bank. The Galicia Bank contains a series of isolated seamounts along its southern edge and is separated from Iberia by a broad submarine valley. The Iberia Abyssal Plain lies south of Galicia Bank (Fig. 2). Here the continental margin has a straight narrow shelf and a steep continental slope. South of 40°N the slope is cut by numerous deep canyons, and at 39°N the east-west Estremadura Spur separates the Iberia Abyssal Plain from the Tagus Abyssal Plain that forms the southern part of the Iberia continental margin. South of the Tagus Abyssal Plain, the east-northeast Gorringe Bank marks the seismically active plate boundary between Eurasia and Africa.

Three main episodes of Mesozoic rifting marked the separation of the Iberia Margin from the Newfoundland Grand Banks. The first episode was a Triassic to Early Jurassic rifting phase that produced graben and half-graben structures in which evaporites were deposited (Wilson et al., 1989; Murillas et al., 1990). A second rifting event consisted of extension in Late Jurassic time. A third episode of Early Cretaceous extension marked the south-to-north breakup of Iberia from the Grand Banks (Boillot, Winterer, et al., 1988; Whitmarsh et al., 1990; Pinheiro et al., 1992). These studies found that the crust in this region is only about 4 km thick and is underlain everywhere by a continuous layer with a velocity near 7.6 km/s that probably is serpentinized mantle peridotite. Plate reconstructions of Iberia with Europe and North America are difficult because Iberia alternately was attached to Europe and Africa (Srivastava et al., 1990).

Leg 149 was designed, on the basis of geophysical data, to drill across the entire OCT from the oceanic to the continental edge of the Iberia rifted margin but instead found an ocean-continent gap at least 130 km wide. Geophysical studies by Whitmarsh et al. (1990), Beslier et al. (1993), and Whitmarsh et al. (1993) have defined the crustal characteristics used to target drill sites on the Iberia Abyssal Plain. The major drill targets on the Iberia Abyssal Plain were a series of basement highs (Fig. 3) beneath several hundred meters of sediment cover. The westernmost basement high drilled is a north-south linear ridge of serpentinized peridotite that has been drilled further north on the western margin of the Galicia Bank at Site 637 (Boillot, Winterer, Meyer, et al., 1987) and collected by the French submersible *Nautile* (Boillot et al., 1988). We drilled the southern extension of the peridotite ridge, displaced to the east from the northern segment, at Site 897. At Holes 897C and 897D, which are about 100 m apart, we encountered partially brecciated and veined serpentinized peridotites beneath roughly 686 m of Pleistocene- to Hauterivian-age sediment cover. This geochemical study is designed to constrain the origin of the serpentinized peridotites by determining the major and trace-element compositions of whole-rock samples and a limited number of mineral compositions. Other studies are emphasizing the study of mineral compositions from these rocks (Cornen et al., this volume, chapter 21).

ANALYTICAL TECHNIQUES

A variety of analytical techniques are used because each technique determines certain elements better than others, and by combin-

[1]Whitmarsh, R.B., Sawyer, D.S., Klaus, A., and Masson, D.G. (Eds.), 1996. *Proc. ODP, Sci. Results,* 149: College Station, TX (Ocean Drilling Program).
[2] Department of Geological and Atmospheric Sciences, Iowa State University, Ames, IA 50011, U.S.A. Seifert: kseifert@iastate.edu

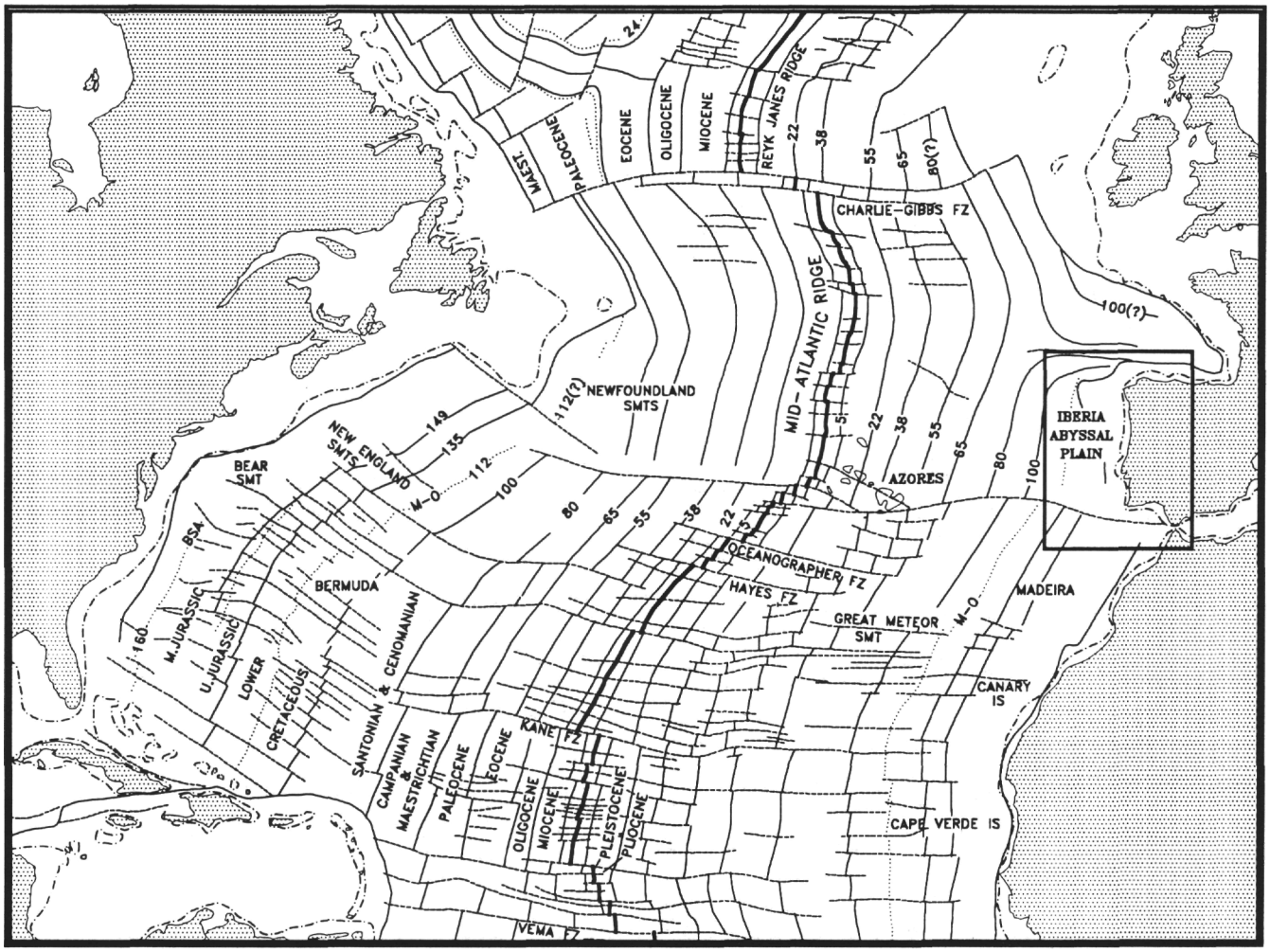

Figure 1. Map of the Atlantic Ocean showing the location of the Iberia Abyssal Plain (box) on the conjugate margin to Newfoundland and the Grand Banks. The map also shows isochrons (m.y.) and fracture zones (dashed lines). Dotted lines denote a few particular magnetic anomalies in the reversal sequence. Modified from Vogt and Perry (1981).

ing techniques we obtain an accurate analysis of many elements. Analysis of these ultramafic rocks was difficult because of the low abundance of many elements and the difficulty of dissolving spinel. Major elements Si, Ti, Al, Fe, Mn, Mg, Ca, Na, K, and P were determined by inductively coupled plasma (ICP) techniques. The oxidation state of Fe required a separate titration, and H_2O^+, H_2O^-, and CO_2 have been lumped into loss on ignition (LOI). Trace elements Ba, V, Cr, Ni, Zn, Cu, Pb, and Sr also were determined by ICP analysis. Fourteen rare-earth elements (REEs), Sr, Ba, Th, Rb, Nb, Y, Hf, Ta, U, Pb, and Cs were determined by inductively coupled plasma mass spectrometry (ICP/MS). All of the analyses have been contracted out, except for the ferrous iron titrations, which were done at Iowa State University. ICP analyses were obtained from commercial laboratories (Chemex and Acme), and ICP/MS analyses were obtained from the GeoAnalytical Laboratory at Washington State University. Charles Knaack was the ICP/MS analyst. Accuracy of the ICP analyses was checked by including United States Geologic Survey standards BCR-1 and BHVO-1 and NBS flyash 1633a as unknowns among the samples and by repeated runs of the commercial laboratory in-house standards. Accuracy of the ICP/MS analyses was checked by a well-characterized BCR-1 clone from the same quarry (BCR-P) and other in-house standards used at the Washington State GeoAnalytical Laboratory. Precision of both the ICP and ICP/MS analyses was estimated at 5% to 10% from duplicate runs of standards and several unknowns, except near the detection limit, which was 0.1 to 0.5 chondrite for trace elements run by ICP/MS. Trace elements run by both ICP and ICP/MS appear to have been more accurately determined by ICP/MS analysis, and the ICP/MS data are preferentially reported. Mineral compositions were determined with the Iowa State University electron microprobe, using well-analyzed mineral standards obtained from various sources.

DESCRIPTION

Petrology

The mantle peridotites drilled at Site 897 are extensively serpentinized, brecciated, and veined, with few fresh minerals remaining. Typically these serpentinized peridotites range from pale green to black with regions containing the rare mineral iowaite exhibiting a bluish cast. The weathered upper part of the serpentinites, and overlying serpentinite fragments in sediments, are highly oxidized and hydrated to a yellow-orange color and contain abundant calcite. Zones of yellow-orange to brown serpentinite occur locally within the green serpentinized peridotite basement near the upper contact

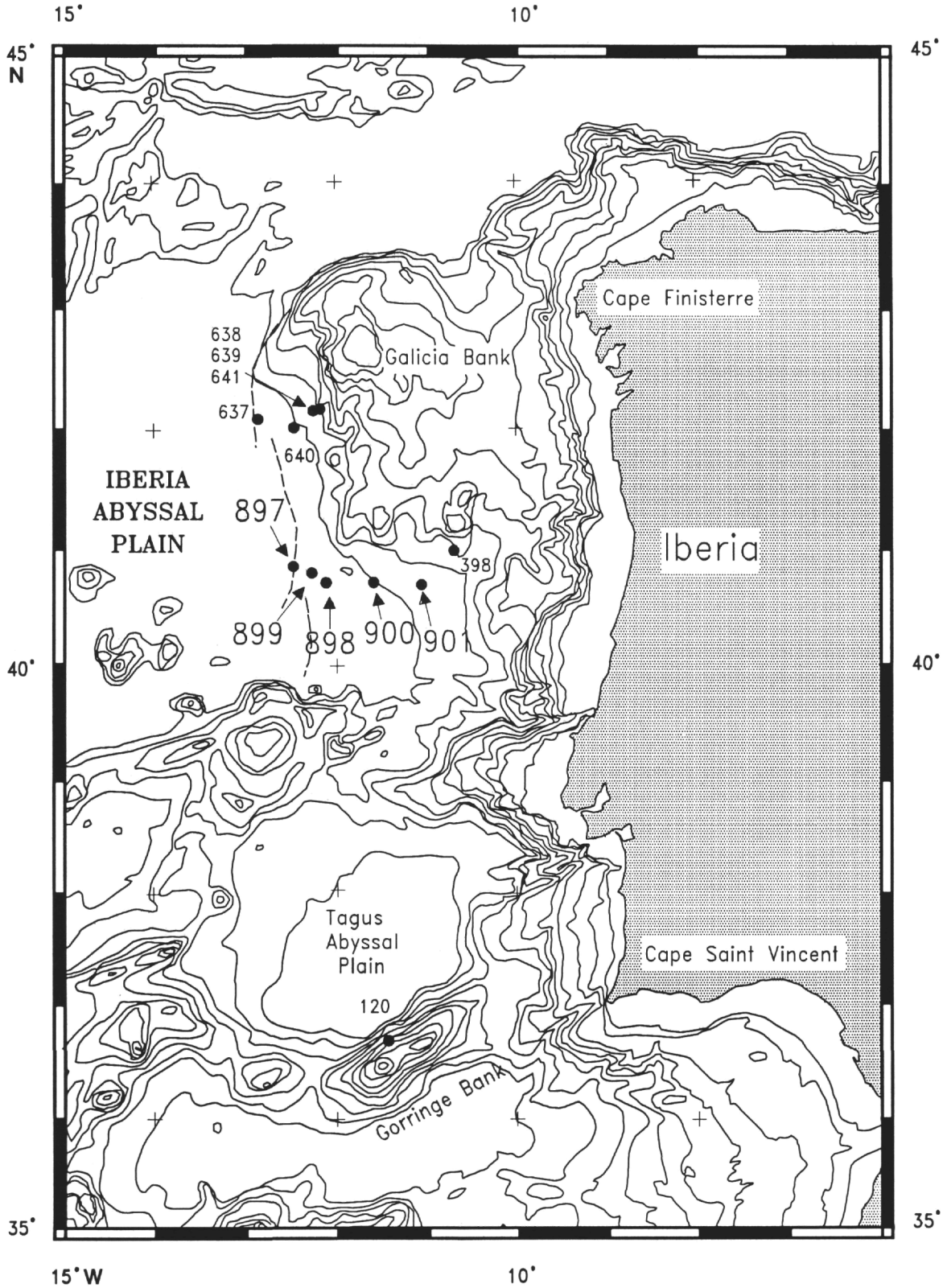

Figure 2. A map of the Iberia continental margin showing the location of the Leg 149 traverse and drill sites on the Iberia Abyssal Plain. Previous drill sites also are marked. The peridotite ridge drilled at Site 897, and earlier at Site 637, is marked with a dashed line. Modified from Sawyer, Whitmarsh, Klaus, et al. (1994).

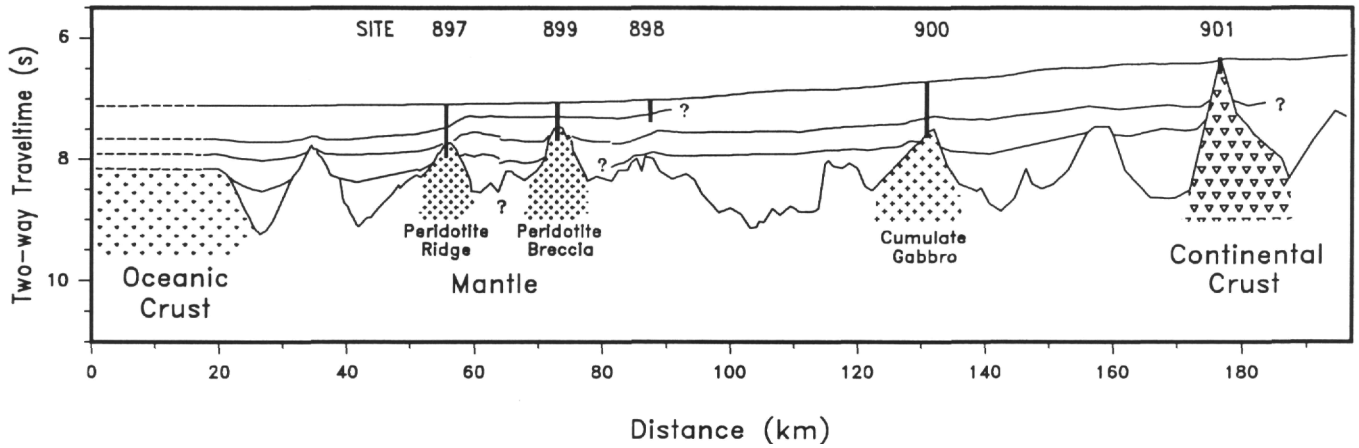

Figure 3. A roughly east-west geologic cross section across the Iberia Abyssal Plain showing the topography of the basement highs drilled on Leg 149 and located on Figure 2. Vertical exaggeration is 5×. Modified from Sawyer, Whitmarsh, Klaus, et al. (1994).

with sediments, probably indicating zones of fluid penetration along fractures. Several generations of crosscutting serpentinite veins are present and locally abundant in these rocks; sometimes small veins are locally controlled by mineral distribution patterns. Lack of a penetrative deformation during serpentinization allowed preservation of primary textures and estimates of the relative percentages of olivine and pyroxene in less deformed parts of these highly altered peridotites.

The Site 897 serpentinized peridotites can be characterized as an upper zone dominated by lherzolites that are locally rich in plagioclase, clinopyroxene, and spinel and a lower zone dominated by harzburgites locally grading into dunite. This distinction is possible because the different alteration patterns of olivine, pyroxenes, and plagioclase frequently allow estimates of primary mineral percentages. Pyroxene and olivine typically are randomly distributed (Fig. 4), but pyroxene-rich bands, zones, and dikelets are locally abundant. Plagioclase has a very irregular distribution, being absent in most places, but quite abundant in a few zones in the upper part of the section (Fig. 5). Clinopyroxene also has an irregular distribution and frequently is associated with plagioclase. Spinel typically is more abundant in lherzolites but is a ubiquitous accessory mineral in all of the serpentinized peridotites, often being the only fresh primary mineral remaining after the extensive serpentinization and brecciation.

The upper section of Hole 897C contains a larger proportion of relatively fresh lherzolites than the upper section of Hole 897D, and mineral compositions reported are all from large crystals in this part of the section (Table 1). No minerals were analyzed in the more severely altered lower harzburgites and dunites. The best preservation occurs in lherzolites from the upper part of Hole 897C, where large fresh olivine, orthopyroxene, clinopyroxene, plagioclase, and spinel crystals are surrounded by mylonitic bands of small recrystallized plagioclase, clinopyroxene, orthopyroxene, and olivine crystals (Fig. 6A, B). The larger plagioclase crystals cluster around spinel (Fig. 5), less commonly around olivine, whereas smaller plagioclase crystals concentrate in the mylonitic bands with a recrystallized texture. The association of plagioclase with spinel in these rocks might suggest a possible origin from spinel at the spinel/plagioclase phase boundary as the peridotites were being uplifted across the phase boundary. However, the lack of reaction or zoning in either of these minerals indicates they are in equilibrium and suggests that equilibrium occurred at pressures near 0.9 GPa, at depths of approximately 27 km.

The fine-grained bands of recrystallized plagioclase, clinopyroxene, orthopyroxene, and olivine appear to have intruded the fragmented coarser grained peridotite. The concentration of plagioclase and clinopyroxene in these bands of small crystals suggests solidification from an intrusive basaltic magma, which probably formed by melting at greater depth. Recrystallization of the fine-grained bands of basaltic material is most likely to have occurred shortly after solidification while the temperature remained high (Fig. 6C). However, plagioclase compositions cluster near an extremely calcic An_{91} Ab_9 Or_0 in both fine-grained recrystallized bands and in adjacent larger plagioclase crystals, indicating that equilibrium has been obtained between the small and large plagioclase crystals. None of the plagioclase crystals show zoning, and we can not explain their calcic nature. Reaction temperatures between 1206° and 1230°C were calculated from a large clinopyroxene crystal with exsolved orthopyroxene lamella in Core 149-897C-64R, similar to Figure 6D, and from adjacent crystals in two Core 149-897C-67R samples (Table 1) using the two-pyroxene formula of Wells (1977) and the method of Wood and Banno (1973). Similar calculations using clinopyroxene and orthopyroxene from the smaller recrystallized bands yield a temperature near 1170°C, only slightly lower than the coarser material, suggesting equilibrium and recrystallization during a single prolonged event.

Iowaite occurs primarily as zones of disseminated crystals and in one large, bright blue-purple concentration of crystals adjacent to a brucite vein in the first few centimeters of Section 149-897D-17R-6 in serpentinized peridotite. The brucite-iowaite association in this sample supports the assumption that iowaite can form from brucite by taking chlorine into its structure to neutralize an oxidized iron ion in brucite (Heling and Schwarz, 1992). The bluish color faded over time into a dull gray as exposed iowaite dehydrated when exposed to the atmosphere. When patches of iowaite were examined under the bright light of a binocular microscope, the color could be observed to fade within minutes, indicating extreme instability at even slightly elevated temperature. Iowaite was identified on Leg 149 through the identification of its two large peaks on X-ray diffraction (XRD) patterns by Kitty Milliken, Ian Gibson, and the first author. Iowaite was first observed in an altered serpentinite associated with low-temperature-alteration minerals from drill core in northwestern Iowa by Kohls and Rodda (1967). The crystal structure was further defined by Allman and Donnay (1969) and it has been reported from drill core of serpentinite in Russia and from drill core of serpentinite muds from ODP Leg 125 by Heling and Schwarz (1992). The occurrence of iowaite XRD patterns correlates with the abundance of Cl in serpentinite cores, exceeding 1% in Sample 149-897C-71R-3, 57-59 cm (Gibson et al., this volume), and a bluish color in hand specimens. All known occurrences of iowaite are from drill cores, further attesting to its instability.

Figure 4. A random distribution of light gray altered pyroxene crystals floating in darker serpentinized olivine in Sample 149-897D-23R-3, 3-17 cm.

Figure 5. Light gray to white altered plagioclase surrounding spinel crystals and, less often, other minerals in serpentinized peridotite in Sample 149-897C-65R-1, 106-115 cm.

Major Element Composition—Hole 897C

Major element ICP data were obtained for all 41 samples chosen for study (Tables 2, 3), but trace-element ICP/MS data were only obtained for 15 of the samples, mostly from Hole 897C. The upper sections of Holes 897C and 897D contain abundant alteration minerals, brecciation, and veining (Milliken et al. this volume). Despite efforts to remove the most conspicuous alteration material by removing the large veins and crystals, much obviously remained in the analyzed cores. Section 149-897C-63R-2, probably a large block of serpentinite in sediments above basement, is dominated by abundant LOI and CaO from abundant secondary calcite (Fig. 7). On the basis of our major element data, Hole 897C can be roughly divided into three parts that have different major element patterns.

The uppermost part of Hole 897C from Section 149-897C-63R-2 to lower Section 149-897C-66R-4 (Fig. 7) can be characterized as variable, partly because of brecciation and late calcite contamination from seawater. As calcite content increases, the concentrations of SiO_2, TiO_2, and Al_2O_3 all decrease significantly, whereas MgO and FeO_t decrease only slightly. Two of the least mobile components, Cr_2O_3 and NiO, concentrate as calcite increases (Gibson et al., this volume; Milliken et al., this volume), indicating they are not being removed by weathering at Site 897. Large Cr_2O_3 concentrations in

Table 1. Major element composition of selected minerals in Hole 897C.

Mineral:	Opx	Host cpx*	Exsol opx*	Bulk xyl*	Olivine	Spinel	Cpx	Opx	Plag	Cpx	Opx	Spinel	Plag
Core, section:	64R-1	64R-1	64R-1	64R-1	67R-3	67R-3	67R-3	67R-3	67R-3	67R-3	67R-3	67R-3	67R-3
Interval (cm):	24–29	24–29	24–29	24–29	12–18	12–18	12–18	12–18	12–18	112–118	112–118	112–118	112–118
Major oxides (wt%)													
SiO_2	54.91	49.64	52.55	49.82	40.49	—	49.85	53.90	44.93	50.14	53.97	0.01	43.66
TiO_2	0.26	0.53	0.08	0.45	0.02	0.38	0.45	0.20	—	0.68	0.28	0.25	—
Al_2O_3	3.06	7.80	6.86	7.06	0.04	39.85	7.08	4.02	35.69	5.98	3.74	47.45	36.17
Cr_2O_3	0.34	0.34	0.28	0.33	—	22.67	0.63	0.63		0.78	0.57	17.56	—
FeO_t	7.85	4.15	8.71	5.01	10.83	21.35	3.78	7.33	0.15	3.55	7.62	17.30	0.13
NiO	0.08	0.04	0.07	0.04	0.34	0.37	0.04	0.06	—	0.03	0.05	0.36	—
MnO	0.21	0.12	0.21	0.14	0.14	0.15	0.10	0.15	0.02	0.08	0.16	0.15	0.03
MgO	31.43	14.70	30.88	17.86	48.83	15.27	15.22	31.26	0.33	15.84	31.62	17.15	0.31
CaO	1.73	22.80	0.46	18.42	0.03	0.04	22.98	1.73	18.13	23.06	2.33	0.03	18.92
Na_2O	0.03	0.43	0.05	0.36	—	0.01	0.39	0.04	1.30	0.36	0.03	0.03	0.93
K_2O	—	0.02	0.02	0.02	—	—	0.01	—	—	0.01	—	0.01	0.01
Total	99.90	100.57	100.17	99.51	100.72	100.09	100.53	99.32	100.55	100.51	100.37	100.30	100.16

Notes: Opx = orthopyroxene; Host cpx = host clinopyroxene; Exsol opx = exsolved orthopyroxene; Bulk xyl = bulk clinopyroxene crystal; Cpx = clinopyroxene; Opx = orthopyroxene; Flag = plagioclase. * = Host cpx and exsol opx are from a large cpx crystal with exsolved orthopyroxene; bulk xyl is the total composition using relative percentages. — = abundance below detection limit.

these rocks are caused by concentrations of chrome spinel. It is also interesting to note that the oxidation ratio, Fe_3/Fe_2, does not change significantly as calcite content changes dramatically in the upper part of Hole 897C, indicating that the depositing solutions were not strongly oxidized.

The middle part of Hole 897C includes only lherzolites from Core 149-897C-67R, and they are enriched in TiO_2, Al_2O_3, CaO, and Cr_2O_3, reflecting an enrichment in plagioclase, clinopyroxene, and chrome spinel relative to the lower part of this hole. Below the upper calcite-rich zone, compositional variations are caused largely by variations in the mineralogy of Hole 897C cores. This middle part of the core has the lowest NiO content and relatively low MgO and FeO_t indicating a relatively low abundance of olivine. Nevertheless, the middle-core lherzolites contain olivine and are characterized by a mineral assemblage that includes olivine, orthopyroxene, clinopyroxene, plagioclase, and spinel (Table 1). Although these minerals typically are in various stages of alteration, they represent the least altered cores recovered at Site 897.

The lower part of Hole 897C includes only harzburgites from Core 149-897C-71R-1, and they are enriched in MgO and NiO, reflecting an enrichment in olivine relative to the upper parts of Hole 897C. Mineralogically this lower core consists largely of serpentinized olivine and orthopyroxene with minor spinel. The NiO will be concentrated in the poorly serpentinized olivine. As LOI increases in the lower part of Hole 897C so does the oxidation ratio Fe_3/Fe_2, correlating with the increase of magnetite associated with serpentinization. The low values of TiO_2, Al_2O_3, and CaO in the lower part of Hole 897C indicate that clinopyroxene and plagioclase are not present, correlating with thin-section observations.

Throughout Hole 897C, TiO_2, Al_2O_3, Cr_2O_3, FeO_t, and CaO roughly correlate, suggesting a correlation between the abundance of plagioclase, clinopyroxene, and spinel. These oxides anticorrelate with NiO, MgO, LOI, and Fe_3/Fe_2, which roughly correlate with each other and the abundance of olivine. The abundance of orthopyroxene is more difficult to assess from compositional data. The better anticorrelation of NiO than MgO with Al_2O_3 and TiO_2 suggests that orthopyroxene abundance is variable and makes compositional correlations more difficult.

Major Element Composition—Hole 897D

The upper section from Hole 897D, consisting of Cores 149-897D-19R and 20R, is relatively brecciated and variable in composition compared to the rather uniformly depleted lower section downward from Core 149-897D-21R to the bottom of the hole (Fig. 8). The lower depleted section from this hole is more depleted than the lower section of Hole 897C and contains a larger proportion of dunites. The upper section of this hole also is dominated by lherzolites and, consequently, is more enriched in TiO_2, Al_2O_3, and Cr_2O_3 than the lower section. However, plagioclase and clinopyroxene are less abundant and less fresh in the upper part of this hole than in the upper part of Hole 897C. The difference in mineralogy between holes is illustrated by the difference in the magnitude of the values used for scale for the various oxides in Figures 7 and 8. In Hole 897C, CaO, Al_2O_3, and TiO_2 have larger abundances and higher magnitude scale values (Fig. 7) whereas in Hole 897D, MgO and NiO have greater abundances and higher magnitude scale values (Fig. 8). There is a slightly greater LOI content in the upper part of Hole 897D than in the lower part, but oxidation is greater in the lower part of the hole. TiO_2, Al_2O_3, and Cr_2O_3 correlate well with each other and anticorrelate with MgO and NiO. This anticorrelation is especially evident in Section 149-897D-20R-3 (Fig. 8), where large peaks in TiO_2 and Al_2O_3, and a small peak in CaO, anticorrelate with negative peaks in MgO and NiO, suggesting olivine is depleted relative to plagioclase and clinopyroxene but not spinel; Cr_2O_3 is not strongly enriched. MgO and NiO correlate poorly with each other because of a variable orthopyroxene content. Although pyroxene-rich and -poor zones alternate in some parts of Hole 897D, these zones were not sampled.

Trace Elements

Trace-element ICP/MS data are available for only 15 of the 41 samples analyzed, mostly from Hole 897C but also some from Core 149-897D-19R (Table 2); trace-element data will not be considered separately for the two holes. Lherzolites are more enriched in incompatible trace elements than are harzburgites and dunites, and they exhibit two distinct types of REE patterns. The first type of REE pattern is roughly flat with an abundance near chondritic, as illustrated by Sample 149-897C-66R-4, 61-63 cm (Fig. 9). The second type of lherzolites REE pattern is similar to normal mid-ocean ridge basalt (N-MORB) with depleted light rare-earth elements (LREE) and flat heavy rare-earth elements (HREE) near 2× to 7× chondrite, as illustrated by Sample 149-897C-67R-1, 33-36 cm (Fig. 10). Both types of lherzolite REE patterns are enriched relative to the flat REE pattern at an abundance of only 0.1× chondrite shown by depleted harzburgite from Core 149-897C-71R (Fig. 11). The REE patterns for the few Hole 897D lherzolites analyzed are similar to Sample 149-897C-66R-4, 61-63 cm, pattern with HREE near chondritic, but with depleted LREE (Fig. 12). The flat REE pattern for Sample 149-897C-66R-4, 61-63 cm (Fig. 9), is close to the 2× chondrite abundance often regarded as typical of undepleted mantle. The N-MORB REE pattern of Sample 149-897C-67R-1, 33-36 cm (Fig. 10), is not

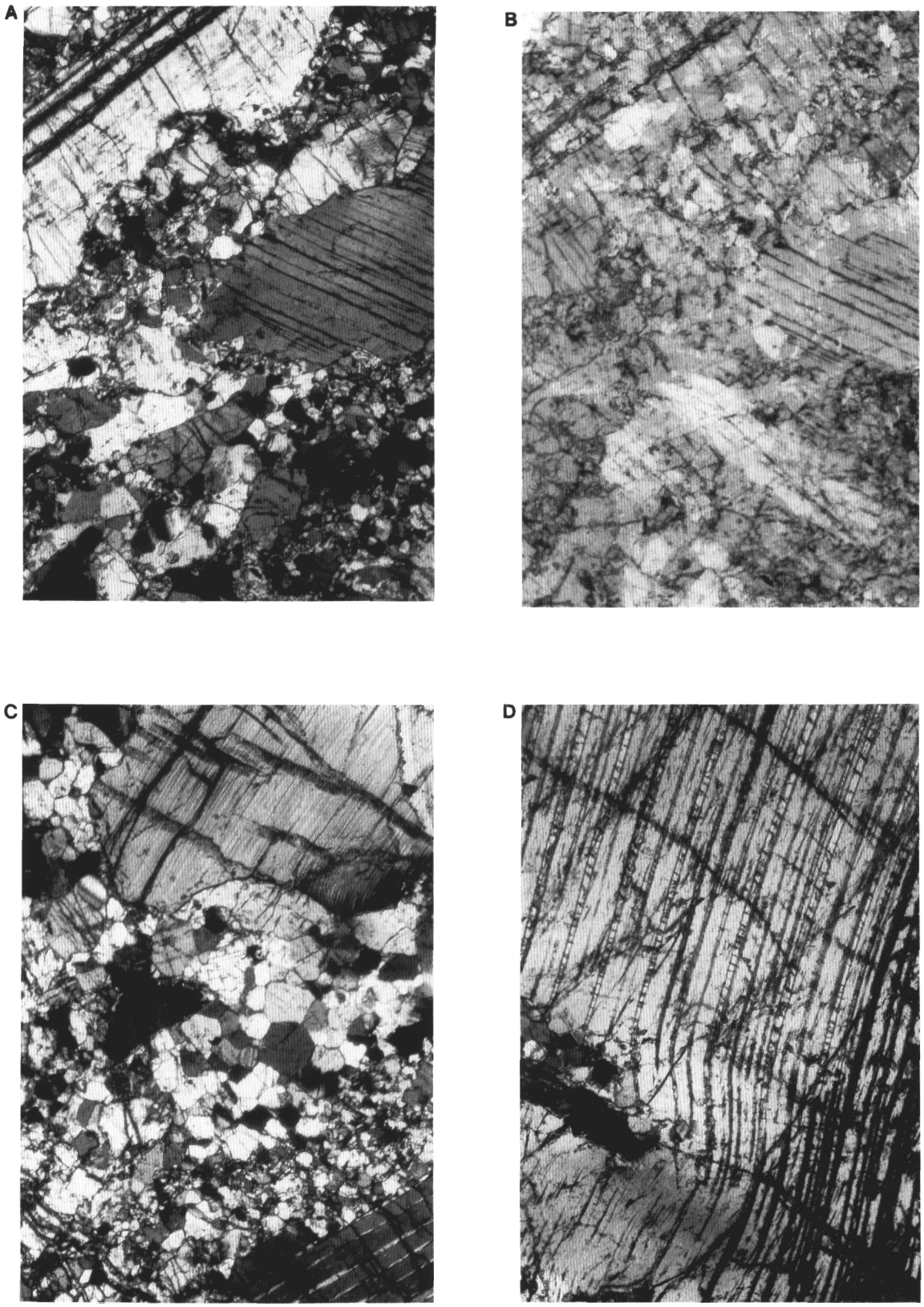

Figure 6. Photomicrographs of Sample 149-897C-66R-4, 55-57 cm, with a long dimension of approximately 2.7 mm. **A.** Bands of small recrystallized material between and around large crystals of pyroxene (gray with black lamellae) and plagioclase (white with black lamellae) in cross-polarized light (XPL). **B.** Same area in plane-polarized light (PPL). **C.** Coarsely recrystallized material between larger crystals of orthopyroxene (light gray) and clinopyroxene (dark gray with white lamella) in XPL. **D.** Large clinopyroxene crystal with exsolved lamellae of orthopyroxene marked with small dark cross-lamellae in XPL.

Table 2. Major and trace-element composition of selected Site 897 serpentinized peridotites.

Hole:	897C	897C	897C	897C	897C	897C	897C	897C	897C	897C	897C	897C	897D	897D	897D
Section, core:	65R-2	66R-4	66R-4	67R-1	67R-1	67R-2	67R-3	67R-3	71R-1	71R-2	71R-3	72R-1	19R-1	19R-1	19R-1
Interval (cm):	65–74	30–40	61–63	24–27	33–36	45–50	12–18	56–60	108–113	55–60	27–36	16–23	42–44	95–101	116–120
Major oxides (wt%)															
SiO_2	36.41	36.14	38.85	37.46	33.28	41.49	42.68	42.71	33.24	32.85	33.75	34.24	33.16	31.50	30.86
TiO_2	<.01	0.05	0.11	0.21	0.20	0.17	0.11	0.15	0.01	0.01	0.02	0.02	0.03	0.08	0.09
Al_2O_3	0.66	2.36	14.43	9.33	8.72	6.20	8.51	8.78	0.39	0.56	0.49	0.47	1.89	6.72	3.52
Cr_2O_3	0.26	0.37	0.15	0.32	0.34	0.49	0.45	0.50	0.23	0.24	0.23	0.32	0.33	0.35	1.02
Fe_2O_3	1.73	4.10	1.45	1.71	1.83	1.36	1.63	1.75	3.81	3.99	4.43	4.23	2.56	2.42	1.46
FeO	5.07	3.43	4.22	3.72	3.10	4.18	5.03	5.41	2.31	2.06	2.18	2.31	3.65	2.97	2.64
MnO	0.14	0.11	0.12	0.14	0.13	0.09	0.11	0.12	0.09	0.08	0.09	0.10	0.09	0.13	0.09
MgO	32.67	39.50	22.95	31.22	36.81	32.22	27.90	27.34	41.02	41.30	41.77	40.78	40.51	38.64	40.49
NiO	0.22	0.22	0.09	0.09	0.08	0.10	0.15	0.14	0.21	0.20	0.22	0.22	0.21	0.12	0.10
CaO	5.32	0.23	7.67	2.46	1.35	2.62	5.04	5.65	0.04	0.08	0.07	0.04	0.13	0.12	0.24
Na_2O	0.13	<.01	0.27	0.14	0.01	0.06	0.44	0.34	0.04	0.18	0.05	0.06	0.10	0.03	0.13
K_2O	0.10	0.07	0.29	0.12	<.05	<.05	0.12	<.05	<.05	0.15	<.05	<.05	0.10	<.05	<.05
P_2O_5	0.08	0.09	0.05	0.07	0.05	0.06	0.05	0.07	0.07	0.09	0.11	0.08	0.09	0.09	0.08
LOI	15.70	13.60	8.60	12.20	13.60	10.00	6.80	6.00	18.20	18.40	16.00	16.80	16.80	16.20	18.80
TOTAL	98.49	100.27	99.25	99.19	99.50	99.04	99.02	98.96	99.66	100.19	99.41	99.67	99.65	99.37	99.52
FeOt	6.63	7.13	5.53	5.26	4.75	5.41	6.50	6.98	5.74	5.65	6.17	6.12	5.96	5.15	3.95
Fe_3/Fe_2	0.34	1.20	0.34	0.46	0.59	0.33	0.32	0.32	1.65	1.94	2.03	1.83	0.70	0.81	0.55
Trace elements (ppm)															
La	0.53	0.05	0.36	0.10	0.08	0.14	0.12	0.46	0.08	0.04	0.02	0.08	0.03	0.09	0.05
Ce	0.61	0.17	0.63	0.42	0.36	0.38	0.35	0.92	0.14	0.08	0.05	0.13	0.09	0.38	0.33
Pr	0.09	0.03	0.14	0.13	0.13	0.11	0.11	0.15	0.02	0.01	—	0.02	0.03	0.09	0.08
Nd	0.30	0.19	0.74	1.06	1.03	0.79	0.68	0.91	0.07	0.05	0.03	0.07	0.18	0.51	0.61
Sm	0.11	0.09	0.34	0.70	0.67	0.43	0.33	0.49	0.03	0.02	0.02	0.02	0.09	0.27	0.31
Eu	0.05	0.04	0.18	0.32	0.32	0.18	0.15	0.22	0.01	0.01	0.01	—	0.05	0.12	0.11
Gd	0.18	0.13	0.49	1.13	1.06	0.59	0.43	0.80	0.02	0.03	0.01	0.02	0.16	0.43	0.48
Tb	0.04	0.03	0.11	0.26	0.25	0.13	0.09	0.17	—	—	—	—	0.04	0.10	0.11
Dy	0.24	0.17	0.68	1.84	1.86	0.85	0.59	1.19	0.03	0.03	0.02	0.03	0.26	0.71	0.83
Ho	0.06	0.04	0.14	0.42	0.42	0.18	0.13	0.24	0.01	0.01	0.01	0.01	0.06	0.15	0.19
Er	0.19	0.13	0.39	1.26	1.25	0.53	0.37	0.63	0.02	0.02	0.02	0.02	0.16	0.44	0.54
Tm	0.03	0.01	0.05	0.18	0.18	0.07	0.05	0.08	—	—	—	—	0.02	0.06	0.08
Yb	0.18	0.11	0.33	1.16	1.13	0.50	0.34	0.53	0.02	0.03	0.02	0.02	0.15	0.39	0.46
Lu	0.03	0.02	0.05	0.18	0.18	0.08	0.05	0.08	—	0.01	—	0.01	0.02	0.06	0.07
Y	2.15	0.88	3.50	10.6	10.2	4.70	3.44	5.93	0.14	0.22	0.13	0.14	1.47	3.98	4.75
Th	0.04	0.02	0.04	0.01	0.01	0.01	0.01	0.06	0.01	0.01	—	0.03	—	0.02	—
Nb	0.07	0.06	0.08	0.04	0.04	0.10	0.06	0.13	0.07	0.04	0.05	0.05	0.06	0.06	0.05
Hf	0.03	0.04	0.14	0.24	0.27	0.17	0.14	0.24	0.02	0.02	0.02	0.01	0.05	0.1	0.07
Ta	—	—	0.01	—	—	—	—	—	—	—	—	—	0.02	—	—
U	—	0.01	0.01	—	0.01	—	—	0.01	—	—	—	—	—	—	—
Pb	0.20	0.06	0.12	0.05	0.44	0.35	0.13	0.08	0.07	0.06	0.13	0.10	0.08	0.17	0.08
Ba	1.6	0.4	19	2.3	2.2	3.8	3.4	3.0	2.4	2.0	1.4	2.6	0.2	1.0	0.4
Sr	26	2.5	199	97	46	34	211	54	4.7	7.8	4.9	4.8	6.6	5.5	6.6
Rb	0.15	0.07	0.73	0.17	0.12	0.34	0.27	0.46	0.13	0.04	0.02	0.35	0.14	0.23	0.2
Cs	0.01	—	0.03	0.01	0.01	0.01	0.02	0.03	—	—	—	0.01	—	0.01	—
Zn	50	46	36	33	31	35	49	75	34	36	37	34	45	39	31
Co	92	98	59	48	43	55	75	80	83	81	88	91	86	57	46
Sc	6	10	25	35	33	26	19	23	5	7	6	5	8	24	23

Note: — = abundance below detection limit.

regarded as typical of undepleted mantle peridotite and suggests metasomatic enrichment by an N-MORB magma.

CONCLUSIONS

The vertical and lateral heterogeneity of the Site 897 serpentinized peridotites is best explained by the separation, movement, and intrusion of basaltic magma. Vertical heterogeneity is caused largely by a greater abundance of lherzolites in the upper section of the Site 897 serpentinized peridotites relative to a lower section consisting largely of depleted harzburgites and dunites. Lateral heterogeneity is caused by a greater abundance of plagioclase-rich lherzolite in the upper part of Hole 897C relative to the upper section of Hole 897D. These variations in peridotite composition can be explained by melting of upward-bulging mantle at depth, separation of the basaltic magma, and selective trapping of the upward-moving magma by cooler portions of the mantle closer to the surface. This process would produce a mantle section with an upper part consisting of fertile lherzolite and a lower part consisting of depleted harzburgite, similar to the Site 897 mantle section. Forming fertile or enriched mantle by the intrusion of basaltic magma has been interpreted as a major process in abyssal peridotites containing plagioclase (Dick et al., 1984; Dick, 1989) and even as a dominant process relative to partial melting (Elthon, 1992) in controlling chemical variations in the upper mantle. Both textural and compositional evidence exists for magma metasomatism in the Site 897 peridotites. The Hole 897C lherzolites contain textural evidence for magma invasion in the form of fine-grained lenses or bands of fresh basaltic material between coarse-grained pyroxenes and olivine, and compositional evidence in the form of REE patterns similar to N-MORB. Lenses of fine-grained solidified magma in coarse-grained peridotite support the movement of magma through the mantle along fractures rather than as a widespread diffusion front along grain boundaries (Kenyon, 1993; Nielson and Wilshire, 1993). Later peridotite-seawater interaction is not likely to change the REE pattern (Menzies et al., 1993; Ridley et al., 1994).

ACKNOWLEDGMENTS

The first author appreciates the opportunity to have been a shipboard petrologist on Leg 149, the guidance and co-operation of Co-Chief scientists Dale Sawyer and Bob Whitmarsh, and the support of an excellent technical staff and facilities on the ship. Data gathering for this study was supported by USSSP Grant No. 0040 to the first author. This manuscript has been greatly improved by the constructive review of Rodey Batiza as well as by the comments of the ODP edi-

torial staff. Most importantly, we are grateful to GeoAnalytical Laboratory analyst Charles Knaap for his careful analyses of these difficult rocks, without which this study would not have been possible.

REFERENCES

Allman, R., and Donnay, J.D.H., 1969. About the structure of iowaite. *Am. Mineral.,* 54:296-299.

Anders, E., and Grevesse, N., 1989. Abundances of the elements: meteoritic and solar. *Geochim. Cosmochim. Acta,* 53:197-214.

Beslier, M.-O., Ask, M., and Boillot, G., 1993. Ocean-continent boundary in the Iberia Abyssal Plain from multichannel seismic data. *Tectonophysics,* 218:383-393.

Boillot, G., Comas, M.C., Girardeau, J., Kornprobst, J., Loreau, J.-P., Malod, J., Mougenot, D., and Moullade, M., 1988. Preliminary results of the Galinaute cruise: dives of the submersible *Nautile* on the Western Galicia Margin, Spain. *In* Boillot, G., Winterer, E.L., et al., *Proc. ODP, Sci. Results,* 103: College Station, TX (Ocean Drilling Program), 37-51.

Boillot, G., Winterer, E.L., et al., 1988. *Proc. ODP, Sci. Results,* 103: College Station, TX (Ocean Drilling Program).

Boillot, G., Winterer, E.L., Meyer, A.W., et al., 1987. *Proc. ODP, Init. Repts.,* 103: College Station, TX (Ocean Drilling Program).

Dick, H.J.B., 1989. Abyssal peridotites, very slow spreading ridges and ocean ridge magmatism. *In* Saunders, A.D., and Norry, M.J. (Eds.), *Magmatism in the Ocean Basins.* Geol. Soc. Spec. Publ. London, 42:71-105.

Dick, H.J.B., Fisher, R.L., and Bryan, W.B., 1984. Mineralogic variability of the uppermost mantle along mid-ocean ridges. *Earth Planet. Sci. Lett.,* 69:88-106.

Elthon, D., 1992. Chemical trends in abyssal peridotites: refertilization of depleted suboceanic mantle. *J. Geophys. Res.,* 97:9015-9025.

Heling, D., and Schwarz, A., 1992. Iowaite in serpentinite muds at Sites 778, 779, 780, and 784: a possible cause for the low chlorinity of pore waters. *In* Fryer, P., Pearce, J.A., Stokking, L.B., et al., *Proc. ODP, Sci. Results,* 125: College Station, TX (Ocean Drilling Program), 313-323.

Kenyon, P.M., 1993. Trace elements in migrating high-temperature fluids: effects of diffusive exchange with the adjoining solid. *J. Geophys. Res.,* 98:22007-22020.

Kohls, D.W., and Rodda, J.L., 1967. Iowaite, a new hydrous magnesium hydroxide-ferric oxychloride from the Precambrian of Iowa. *Am. Mineral,* 52:1261-1271.

Menzies, M.A., Long, A., Ingram, G., Tatnell, M., and Janecky, D., 1993. MORB peridotite-sea water interaction: experimental constraints on the behaviour of trace elements, $^{87}Sr/^{86}Sr$ and $^{143}Nd/^{144}Nd$ ratios. *In* Prichard, H.M., Alabaster, T., Harris, N.B.W., and Neary, C.R. (Eds.), *Magmatic Processes and Plate Tectonics.* Geol. Soc. Spec. Publ. London, 76:309-322.

Murillas, J., Mougenot, D., Boillot, G., Comas, M.C., Banda, E., and Mauffret, A., 1990. Structure and evolution of the Galicia Interior basin (Atlantic western Iberian continental margin). *Tectonophysics,* 184:297-319.

Nielson, J.E., and Wilshire, H.G., 1993. Magma transport and metasomatism in the mantle: a critical review of current geochemical models. *Am. Mineral,* 78:1117-1134.

Pinheiro, L.M., Whitmarsh, R.B., and Miles, P.R., 1992. The ocean-continent boundary off the western continental margin of Iberia, II. Crustal structure in the Tagus Abyssal Plain. *Geophys. J.,* 109:106-124.

Ridley, W.I., Perfit, M.R., Jonasson, I.R., and Smith, M.F., 1994. Hydrothermal alteration in oceanic ridge volcanics: a detailed study at the Galapagos fossil hydrothermal field. *Geochim. Cosmochim. Acta,* 58:2477-2494.

Sawyer, D.S., Whitmarsh, R.B., Klaus, A., et al., 1994. *Proc. ODP, Init. Repts.,* 149: College Station, TX (Ocean Drilling Program).

Srivastava, S.P., Schouten, H., Roest, W.R., Klitgord, K.D., Kovacs, L.C., Verhoef, J., and Macnab, R., 1990. Iberian plate kinematics: a jumping plate boundary between Eurasia and Africa. *Nature,* 344:756-759.

Vogt, P.R., and Perry, R.K., 1981. North Atlantic Ocean: bathymetry and plate tectonic evolution. *Geol. Soc. Am., Map and Chart Ser.,* MC-35.

Wells, P.R.A., 1977. Pyroxene thermometry in simple and complex systems. *Contrib. Mineral. Petrol,* 62:129-139.

Whitmarsh, R.B., Miles, P.R., and Mauffret, A., 1990. The ocean-continent boundary off the western continental margin of Iberia, I. Crustal structure at40°30'N. *Geophys. J. Int.,* 103:509-531.

Whitmarsh, R.B., Pinheiro, L.M., Miles, P.R., Recq, M., and Sibuet, J.C., 1993. Thin crust at the western Iberia ocean-continent transition and ophiolites. *Tectonics,* 12:1230-1239.

Wilson, R.C.L., Hiscott, R.N., Willis, M.G., and Gradstein, F.M., 1989. The Lusitanian Basin of west-central Portugal: Mesozoic and Tertiary tectonic, stratigraphic and subsidence history. *In* Tankard, A.J., and Balkwill, H.R. (Eds.), *Extensional Tectonics and Stratigraphy of the North Atlantic Margins.* AAPG Mem., 46:341-361.

Wood, B.J., and Banno, S., 1973. Garnet-orthopyroxene and orthopyroxene-clinopyroxene relationships in simple and complex systems. *Contrib. Mineral. Petrol,* 42:109-124.

Date of initial receipt: 1 December 1994
Date of acceptance: 27 April 1995
Ms 149SR-216

Table 3. Major element composition of selected ODP Site 897 serpentinized peridotites.

Hole:	897C	897C	897C	897C	897C	897D	897D	897D	897D	897D	897D	897D	897D
Core, section:	63R-2	64R-5	64R-5	72R-1	72R-2	19R-2	19R-4	19R-5	20R-1	20R-2	20R-3	21R-1	21R-2
Interval (cm):	112–118	0–11	90–93	102–112	113–123	89–98	114–116	107–113	64–71	88–94	5–8	34–39	42–48
Major oxides (wt%)													
SiO_2	25.84	32.44	47.28	33.31	33.74	33.28	33.75	36.97	35.58	35.40	34.47	33.76	33.82
TiO_2	<.01	0.11	0.22	<.01	<.01	0.05	0.13	0.09	0.02	0.02	0.15	0.02	<.01
Al_2O_3	0.50	7.85	10.57	0.35	0.57	3.27	7.76	6.93	0.78	0.97	8.91	0.47	0.49
Cr_2O_3	0.36	0.19	0.15	0.26	0.21	0.75	0.94	0.56	0.21	0.20	0.31	0.26	0.23
Fe_2O_3	1.21	1.19	1.87	3.27	3.89	1.89	3.19	2.51	4.46	4.66	2.64	3.77	3.93
FeO	3.88	3.69	3.46	3.14	2.68	3.30	4.40	4.08	2.82	2.75	3.15	2.96	2.43
MnO	0.17	0.13	0.13	0.09	0.09	0.10	0.13	0.12	0.09	0.09	0.14	0.09	0.09
MgO	22.39	25.52	17.90	40.78	40.59	39.93	33.31	31.49	40.48	40.53	33.87	40.36	40.70
NiO	0.19	0.11	0.07	0.23	0.23	0.16	0.18	0.17	0.23	0.22	0.11	0.23	0.21
CaO	21.72	9.87	11.57	0.03	0.04	0.18	0.84	3.88	0.19	0.16	1.10	0.14	0.15
Na_2O	0.10	0.33	0.60	0.05	0.08	0.17	0.10	0.06	0.09	0.09	0.07	0.21	0.27
K_2O	<.05	0.12	0.21	<.05	0.07	0.20	0.17	0.10	<.05	<.05	0.09	<.05	0.08
P_2O_5	0.08	0.08	0.04	0.08	0.08	0.10	0.06	0.06	0.09	0.11	0.09	0.10	0.12
LOI	22.40	17.60	5.20	17.80	17.20	16.00	14.00	12.00	14.40	14.40	14.40	17.20	17.20
Total	98.84	99.23	99.27	99.39	99.47	99.38	98.96	99.02	99.44	99.60	99.50	99.57	99.72
FeO_t	4.97	4.76	5.15	6.08	6.18	5.00	7.27	6.35	6.84	6.95	5.53	6.35	5.97
Fe_3/Fe_2	0.31	0.32	0.54	1.04	1.45	0.57	0.73	0.62	1.58	1.69	0.84	1.27	1.62

Hole:	897D	897D	897D	897D	897D	897D	897D	897D	897D	897D	897D	897D	897D
Core, section:	21R-3	21R-4	23R-1	23R-2	23R-3	23R-5	24R-1	24R-3	24R-4	25R-1	25R-2	25R-4	25R-5
Interval (cm):	62–68	72–78	53–58	66–72	11–17	129–137	49–55	102–108	36–42	42–47	104–110	128–134	89–95
Major oxides (wt%)													
SiO_2	33.87	33.45	32.69	32.48	34.81	35.09	33.64	33.21	32.82	34.61	34.43	34.56	34.67
TiO_2	0.02	0.01	0.02	0.02	0.02	0.01	0.03	0.01	0.01	0.01	0.01	0.01	<.01
Al_2O_3	0.36	0.54	0.24	0.07	0.48	0.72	2.05	0.19	0.64	0.52	0.53	0.67	0.45
Cr_2O_3	0.19	0.30	0.30	0.14	0.26	0.21	0.42	0.15	0.39	0.34	0.32	0.43	0.23
Fe_2O_3	5.20	3.83	4.66	3.92	3.85	4.05	3.99	4.40	4.35	3.26	3.61	2.81	2.76
FeO	1.81	2.59	2.90	3.00	3.01	3.15	3.34	2.99	3.10	3.35	2.95	3.65	3.46
MnO	0.10	0.09	0.09	0.10	0.10	0.10	0.10	0.10	0.11	0.10	0.10	0.10	0.09
MgO	41.40	40.90	41.06	41.13	40.23	40.13	40.16	41.55	41.48	41.00	41.21	41.26	41.53
NiO	0.23	0.22	0.27	0.27	0.23	0.23	0.22	0.26	0.26	0.23	0.23	0.22	0.23
CaO	0.13	0.15	0.11	0.10	0.18	0.19	0.18	0.15	0.15	0.17	0.20	0.23	0.20
Na_2O	0.18	0.22	0.04	0.07	0.08	0.15	0.10	0.05	0.07	0.10	0.03	0.03	0.02
K_2O	<.05	0.09	<.05	<.05	<.05	<.05	0.15	0.09	<.05	0.06	<.05	0.13	<.05
P_2O_5	0.10	0.10	0.09	0.17	0.11	0.11	0.08	0.11	0.11	0.10	0.11	0.10	0.10
LOI	17.00	17.20	17.00	18.40	16.20	15.60	15.20	16.30	16.00	15.80	16.00	15.40	15.80
Total	100.59	99.69	99.47	99.87	99.56	99.74	99.66	99.56	99.49	99.65	99.73	99.60	99.54
FeO_t	6.50	6.04	7.10	6.53	6.48	6.80	6.94	6.95	7.02	6.29	6.20	6.18	5.95
Fe_3/Fe_2	2.87	1.48	1.61	1.31	1.28	1.29	1.19	1.47	1.40	0.97	1.22	0.77	0.80

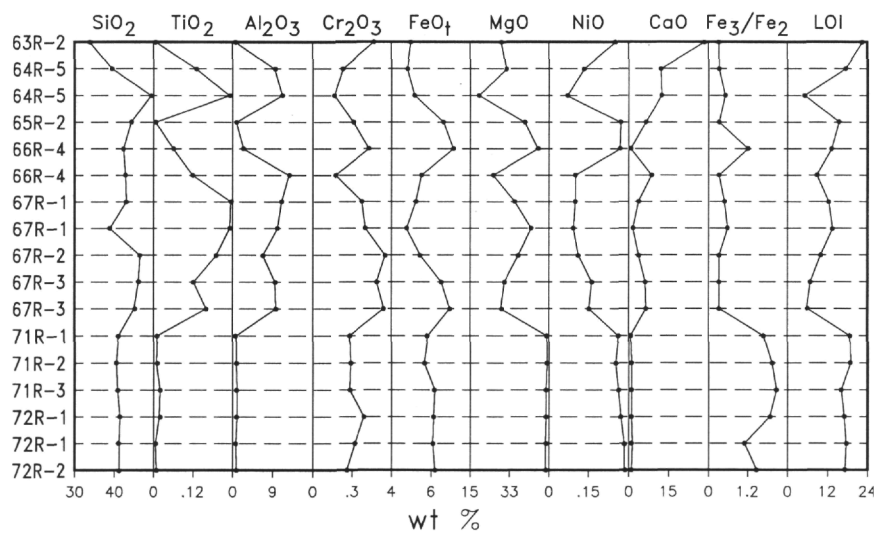

Figure 7. Variation of major element composition (calculated on an anhydrous basis) in the Hole 897C serpentinized peridotites with depth. Fe_3/Fe_2 is the oxidation ratio and shorthand for Fe_2O_3/FeO. The abbreviated core numbers correspond to the samples listed in Tables 2 and 3 and are in order of depth, although spacing between samples is not uniform. The compositional data for this figure are from those tables.

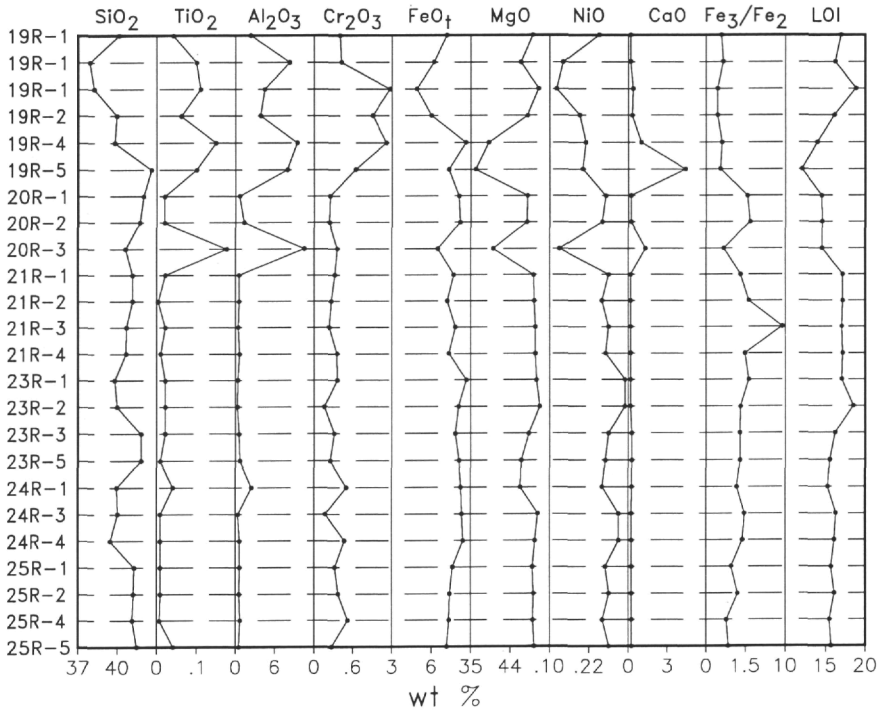

Figure 8. Variation of major element composition (calculated on an anhydrous basis) in the Hole 897D serpentinized peridotites with depth. Fe_3/Fe_2 is the oxidation ratio and shorthand for Fe_2O_3/FeO. The abbreviated core numbers correspond to the samples listed in Tables 2 and 3 and are in order of depth, although spacing between samples is not uniform. The compositional data for this figure are from those tables.

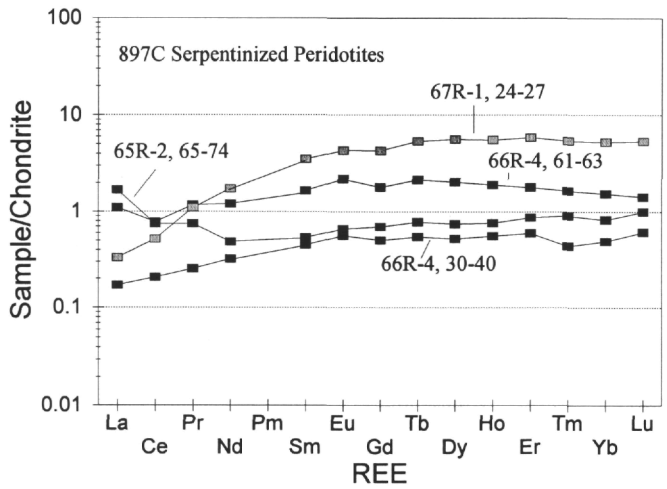

Figure 9. Chondrite-normalized REE patterns for several samples from uppermost basement Cores 149-897C-65R, 66R, and 67R. Peridotite samples from Cores 149-897C-65R and 66R have flat HREE near chondritic abundance, with variable LREE. Sample 149-897C-67R-1, 24-27 cm, has a greater HREE abundance and depleted LREE similar to N-MORB. Chondrite values used for normalization are taken from Anders and Grevesse (1989) and multiplied by 1.36 to maintain consistency with older chondrite normalization values.

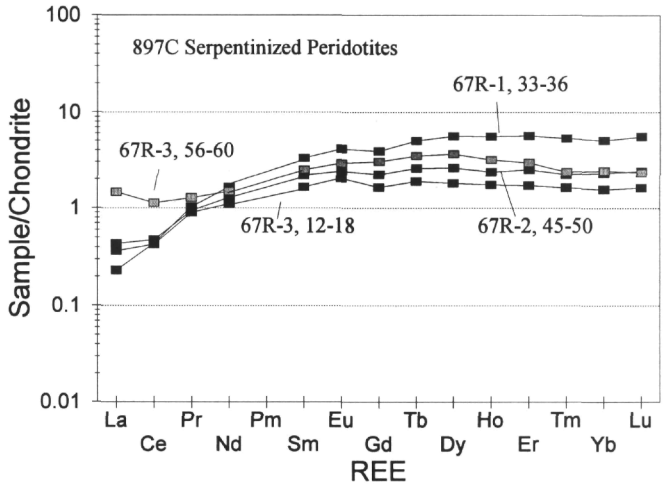

Figure 10. Chondrite-normalized REE patterns for several samples from Core 149-897C-67R showing similarity to N-MORB with HREE near 2× to 7× chondrite and depleted LREE. Elements listed in order of atomic number and normalized as in Figure 9.

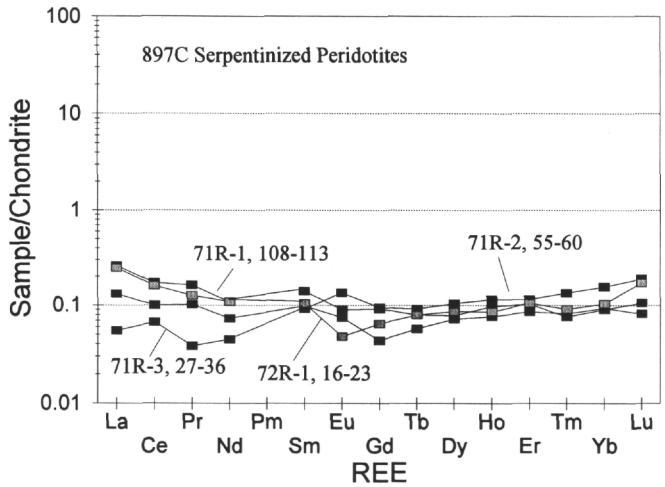

Figure 11. Chondrite-normalized REE patterns for peridotite samples from Core 149-897C-71R. All four samples from this core have relatively flat REE patterns near 0.1× chondrite with variable Eu anomalies and slight enrichment in LREE. This pattern could be interpreted as suggesting some late LREE enrichment superimposed on an earlier LREE depleted pattern. Elements listed in order of atomic number and normalized as in Figure 9.

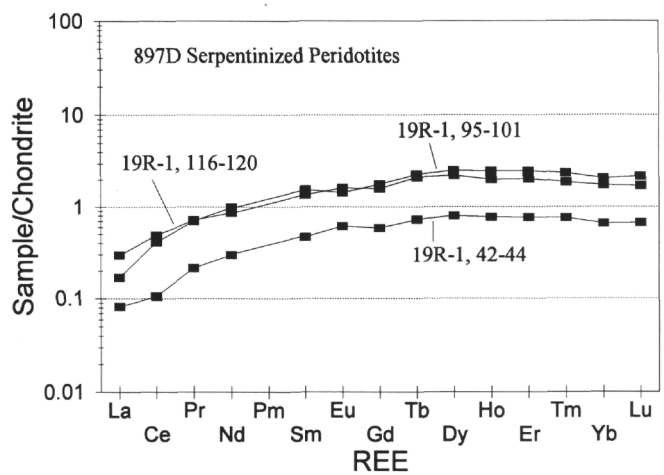

Figure 12. Chondrite-normalized REE patterns for Core 149-897D-19R peridotite samples showing HREE abundance near chondrite and depleted LREE. Elements listed in order of atomic number and normalized as in Figure 9.